ACS APPLIED MATERIALS & INTERFACES

Research Article

www.acsami.org

Nanostructured Proton Conductors Formed via in Situ Polymerization of Ionic Liquid Crystals

Fei Lu,[†] Xinpei Gao,[†] Bin Dong,[‡] Panpan Sun,[†] Nan Sun,[†] Shuting Xie,[†] and Liqiang Zheng*[,†]

[†]Key Laboratory of Colloid and Interface Chemistry, Shandong University, Ministry of Education, Jinan 250100, China

[‡]China Ionic Liquid Laboratory, Dalian Institute of Chemical Physics, Chinese Academy of Science, Dalian 116023, China

Supporting Information

ABSTRACT: Ionic liquid crystals (ILCs) with hexagonal and lamellar phases were successfully fabricated by the self-assembly of a polymerizable amphiphilic zwitterion, which is formed by 3-(1-vinyl-3-imidazolio)-propanesulfonate (VIPS) and 4-dodecyl benzenesulfonic acid (DBSA) based on intermolecular electrostatic interactions. The microstructures and phase behaviors of ILCs were studied by polarized microscope (POM) and small-angle X-ray scattering (SAXS). The ILC topological structures can be considered as proton pathways and further fixed by photopolymerization to prepare nanostructured proton-conductive films. The introduction of highly ordered and well-defined ILC structures into these polymeric films radically improves the ionic conductivities.

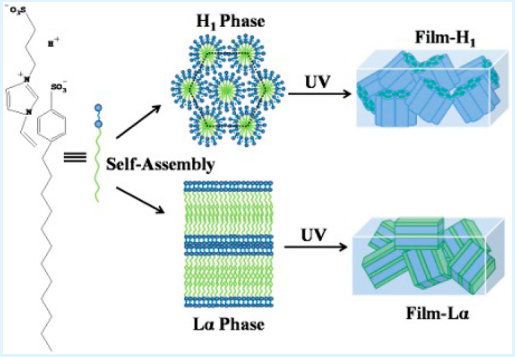

KEYWORDS: *ionic liquid crystals, zwitterions, photopolymerization, proton-conductors, self-assembly*

INTRODUCTION

Fuel cells are electrochemical devices that convert chemical energy to electrical power with high efficiency and large energy density. They can be applied in various fields including portable electronic devices and light electric vehicles.[1,2] As the central elements of fuel cells, proton conductors have gained remarkable interest.[3−6] Perfluorinated sulfonic acid−based polymers such as Nafion are the popular proton conducting membranes due to their good thermal stability and high proton conductivity.[7−9] It is well-known that the phase-separated morphology of Nafion is responsible for the efficient proton-conducting.[10,11] However, the ordered alignment of ionic clusters within Nafion is still limited due to the defined molecular structures. Therefore, the development of a proton conductor with highly ordered structures is necessary for the next generation of fuel cells. Ionic liquid crystals (ILCs) with highly ordered and well-defined self-assembled structures are good candidates.

ILCs, considered as a class of liquid crystalline compounds by ionic species, take advantages of the properties of both ionic liquids (ILs) and liquid crystals (LCs).[12] Our group has previously constructed several ILC systems using pyrrolidinium and imidazolium IL-based surfactants.[13−15] Very recently, Ohno's group has developed the ion-conducting materials on the basis of self-assembly in thermotropic ILCs.[16−18] The introduction of ILCs can significantly improve the ionic conductivity. However, the topological structures of ILCs are extremely dependent on the component concentrations or temperature. Additionally, the low mechanical strength and some deformations of ILCs still restrict a deeper application of these gel electrolytes in practical applications.

Hence, the fixation of ILC nanostructures within a solid polymeric film will make a great progress for the development of ion-transport materials. The construction of nanostructured ILCs based on polymerizable amphiphilic molecules is an efficient approach. Gin and co-workers have achieved a lithium ion conductor based on lyotropic LCs via polymerization.[19] Ohno et al. also designed polymerizable ammonium or imidazolium salts forming thermotropic LCs to prepare ion-conductive polymer films.[20,21] Ivanov et al. synthesized a polymerizable amphiphilic sodium salt to construct ion-conducting polymer membranes with bicontinuous cubic nanostructures.[22] In spite of the remarkable properties of ILCs, the strict requirements on selective transport of target ions are the drawbacks of ILCs in practical cell applications. For example, only protons are the target ions and can be required to conduct in the fuel cells.

To overcome this problem, zwitterions as a covalent combination of cations and anions can be proposed as candidates for the selective target ion transport.[23−26] The zwitterions are expected not to migrate under an applied potential gradient due to the intramolecular neutralized charges. Hence, the applied voltage can only be used to operate the target ions. Several fan-shaped zwitterions have been synthesized in complicated steps and then self-assembled

Received: July 10, 2014
Accepted: December 3, 2014
Published: December 3, 2014

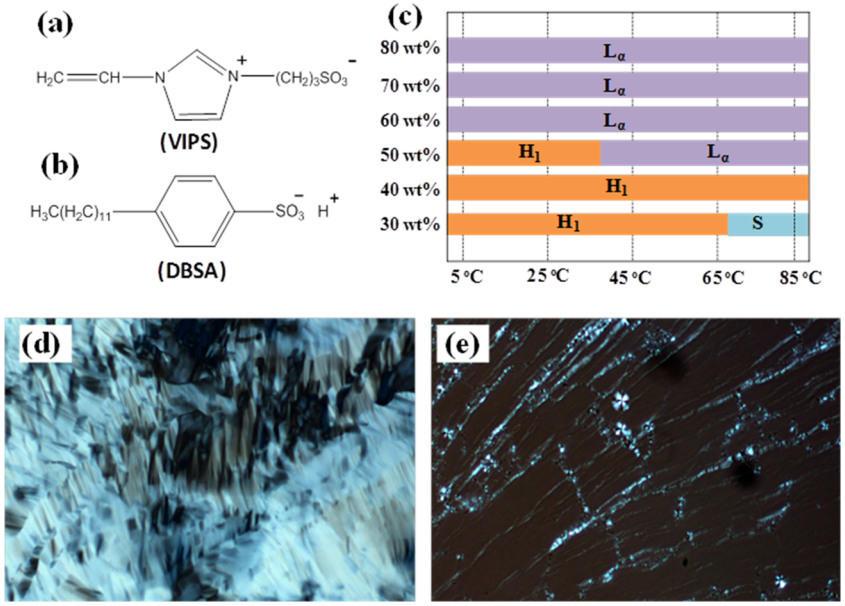

Figure 1. Molecular structures of (a) polymerizable zwitterion 3-(1-vinyl-3-imidazolio) propanesulfonate (VIPS) and (b) 4-dodecyl benzenesulfonic acid (DBSA). (c) Phase diagram of the VIPS−DBSA aqueous mixture. H_1, hexagonal phase; L_α, lamellar phase; S, undefined solution. POM images of (d) 40 and (e) 60 wt % samples at 25 °C.

into ILCs for ion conductors.[27−30] However, to the best of our knowledge, the preparation of proton-transporting polymeric films based on ILCs fabricated by polymerizable zwitterions are still limited. The suitable design of polymerizable zwitterions is a considerate solution for the target ion-transport as well as the fixation of ILC nanostructures.

In the present study, we used a facile method to prepare a polymerizable amphiphilic zwitterion by 3-(1-vinyl-3-imidazolio)propanesulfonate (VIPS) and 4-dodecyl benzenesulfonic acid (DBSA) based on intermolecular electrostatic interactions. According to the hard−soft acid−base theory, the preferential interactions between 4-dodecyl benzenesulfonate anions and the imidazolium cationic part of the zwitterions encourage the formation of zwitterionic amphiphiles with polymerizable moieties.[31] The VIPS−DBSA aqueous mixtures can construct hexagonal and lamellar phases with the increasing component contents. The proton-conductive polymeric films with hexagonal or lamellar nanostructures were successfully derived by photopolymerization of the ILCs. The fixation of the ILC topological structures within the proton-transporting films generates a high ionic conductivity. We expect this work may shed light on the potential of nanostructured proton conductors in practical applications.

EXPERIMENTAL SECTION

Materials. 1-Vinylimidazole (97%) and 4-dodecyl benzenesulfonic acid (95%) were purchased from Sigma-Aldrich. 1,3-Propane sultone (99%) and 2,2-Dimethoxy-2-phenylacetophenone (99%) were the products of J&K Scientific, Ltd. Acetone was obtained from Shanghai Chemical Co. All the materials were used as received without any purification. Deionized water was used throughout all the experiments.

Synthesis of 3-(1-Vinyl-3-imidazolio)propanesulfonate (VIPS). 1-Vinylimidazole (0.1 mol, 9.41 g) was dissolved in 60 mL of acetone. Then, an equimolar amount of 1,3-propane sultone (0.1 mol, 12.24 g) dissolved in 40 mL of acetone was added dropwise to the above solution at 0 °C under a nitrogen atmosphere. The mixture was stirred for 3 days at room temperature. After the reaction, the result solid was filtered and washed with acetone at least three times. Finally, the obtained VIPS was dried under a vacuum at room temperature. The purity of the product was confirmed by ^{1}H NMR. ^{1}H NMR (D_2O, 300 MHz): 9.04 (s, 1H), 7.75 (s, 1H), 7.59 (s, 1H), 7.10 (t, 1H), 5.77 (d, 1H), 5.38 (d, 1H), 4.37 (t, 2H), 2.92 (t, 2H), 2.32 (m, 2H).[32]

Preparation of ILC Phase. The VIPS−DBSA mixture was prepared by weighing all components as designed compositions in weight percent (wt %). VIPS and DBSA were mixed in an equimolar ratio, and the water content varied from 70 to 20 wt %. In detail, appropriate amounts of VIPS−DBSA mixture and water were weighted into a vial, sealed with Parafilm, and homogenized and equilibrated by repeated vortex mixing and centrifugation. Then, each sample was kept at 25 °C for one month before further investigation. It should be noted that the ILC phases are sensitive to water evaporation loss, so each step should be taken to keep the samples sealed as much as possible.

In-Phase Photopolymerization. The photopolymerizable sample was prepared by weighting appropriate amounts of VIPS−DBSA mixture and water into a vial according to the phase diagram. Then, 2,2-dimethoxy-2-phenylacetophenone (2 wt % to the monomer) was added as photoinitiator. After the ILC phase equilibrated, the mixture was sandwiched between two quartz substrates and irradiated by a UV arc lamp with an intensity of 9 mW/cm^2 for 2 h at room temperature from both top and bottom surfaces of the substrates to ensure maximum conversion.

Characterization. The textures of ILC phase were examined by a polarized optical microscope (Zeiss, Axio Scope) equipped with cooled CCD. The temperature was controlled with a Linkam THSME600 liquid crystal freezing and heating stage system with a TP94 temperature controller (Linkam Scientific Instrument Ltd., U.K.). Small-angle X-ray scattering (SAXS) measurements were performed on the SAXSess mc^2 X-ray scattering system (Anton Paar) with a Cu Kα radiation operating at 2 kW (50 kV and 40 mA). The distance between the sample and detector is 264.5 mm, and the wavelength of X-rays is 1.542 Å. The exposure time was 600 s for each sample. The morphologies of the polymeric films were investigated by scanning electronic microscopy (SEM, JEOL JSM-7600F) after gold sputter coating. FT-IR spectra were recorded with a resolution of 2 cm^{-1} using a BIORADFTS-165 spectrometer. Conductivity measurements were carried out by electrochemical impedance spectroscopy in the frequency of 0.1−10^5 Hz with 0.3 mV oscillating voltage using a glass cell consisting of two Pt electrodes and a Teflon spacer.

RESULTS AND DISCUSSION

ILC Phase Behavior and Characterization. The chemical structures of polymerizable imidazole zwitterion VIPS and 4-dodecyl benzenesulfonic acid DBSA are shown in Figure 1a,b. Equimolar amounts of VIPS and DBSA were mixed in aqueous solution with increasing total concentration. A polymerizable amphiphilic zwitterion can be obtained by VIPS and DBSA based on intermolecular electrostatic interactions according to the hard−soft acid−base theory. The temperature−concentration phase diagram of VIPS−DBSA aqueous mixture is shown in Figure 1c. An anisotropic hexagonal phase (H_1) and an anisotropic lamellar phase (L_α) can be constructed with the increasing VIPS−DBSA concentration at 25 °C.

SAXS technique is an efficient method to analyze the details of ILC phases.[33−36] Figure 2 exhibits the SAXS patterns of VIPS−DBSA aqueous mixture with increasing VIPS−DBSA amounts at 25 °C. For the 30, 40, and 50 wt % samples, three scattering peaks in SAXS spectra can be observed. These Bragg peaks with ratio of $1:\sqrt{3}:2$ can be assigned to (100), (110), and (200) reflections of a hexagonal structure for H_1 phase. The nongeometric pattern in POM for hexagonal lattice is also illustrated in Figure 1d. When the VIPS−DBSA concentration increased to 60 wt %, only two Bragg peaks with a relative ratio of 1:2 can be obtained. The two peaks can be indexed as (100) and (200) reflections of a lamellar structure for L_α phase. The oily streaks and Maltese crosses in POM as shown in Figure 1e are the typical textures of L_α phase.

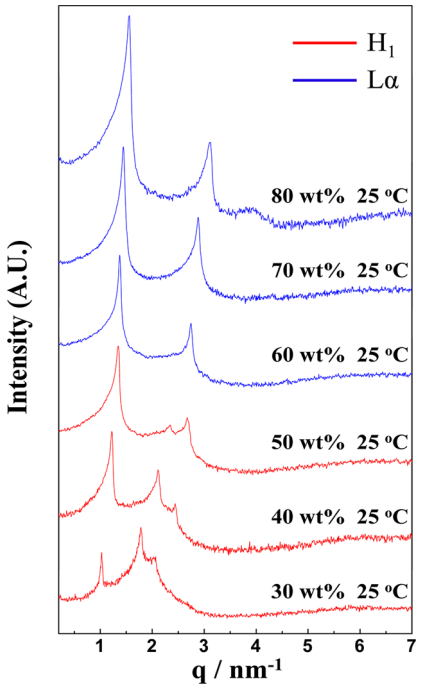

Figure 2. SAXS spectra for the VIPS−DBSA aqueous mixture with increasing concentration of VIPS−DBSA at 25 °C.

The SAXS characterization of ILC phases is based on the periodic order in ILC state. Therefore, the positions of Bragg peaks in SAXS spectra are characteristic for different types of ILC phases. The relevant structure parameters can also be calculated from the SAXS patterns. All the parameters of the VIPS−DBSA systems were deduced from the SAXS results. The corresponding theories and equations, as well as the indexing of the SAXS data, are shown in the Supporting Information. As shown in Table 1, the thickness of water channel (d_w) for the hexagonal phase decreased with the increasing content of VIPS−DBSA. It means the cylinder-like aggregates in H_1 phase pack more densely as the VIPS−DBSA content increases, resulting in a thinner solvent layer. While the radius of cylinder unit (d_H) for the hexagonal phase showed negligible variation with the increasing VIPS−DBSA content. This result suggests that the arrangement of VIPS−DBSA molecules per cylinder-like aggregate is equilibrium at this VIPS−DBSA concentration region. However, the L_α phase shows a different tendency. The thickness of hydrophobic domain (d_L) increases whereas the thickness of water layer (d_w) decreases with an increasing amount of VIPS−DBSA. In other words, as the VIPS−DBSA content in the lamellar phase increases, the water channel is compressed by the expanding surfactant bilayer.

Except for the concentration, temperature is also a key factor for the phase behavior of VIPS−DBSA aqueous mixture. Figure 3 shows the SAXS patterns for 40, 50, and 60 wt % samples. With the temperature increasing from 5 to 85 °C, the 40 and 60 wt % samples gave a hexagonal columnar structure and a lamellar structure, respectively, indicating the thermal stability of the topological structures during this temperature range. For the 50 wt % sample, only hexagonal structural reflection can be observed below 45 °C. When the temperature increased over 45 °C, the Bragg peak assigned to (110) reflection of H_1 phase disappeared gradually, indicating the topological structure turned into L_α phase. The SAXS patterns for 30, 70, and 80 wt % with increasing temperature from 5 to 85 °C are also collected and shown in the Supporting Information. Due to the topological structure in ILC phase is sensitive to temperature and water content, it is pertinent to fix the ILC nanostructure by photopolymerization.

Fixation of ILC Structures by Photopolymerization. The preparation process of nanostructured proton-transporting films is shown in Scheme 1 (more details in the Supporting Information). The hexagonal and lamellar phases were first

Table 1. Structure Parameters for the ILC Phase of VIPS−DBSA Aqueous Mixture[a]

phase	sample wt %	VIPS wt %	DBSA wt %	H_2O wt %	ϕ_L	a_0 (nm)	d_H (nm)	d_L(nm)	d_W (nm)
H_1	30	12.05	17.94	70.01	0.1383	7.042	1.375		4.292
	40	15.98	23.86	60.16	0.1839	5.939	1.337		3.265
	50	19.79	30.71	49.49	0.2368	5.386	1.376		2.633
L_α	60	23.82	36.04	40.14	0.2778	4.574		1.271	3.304
	70	27.95	42.61	29.44	0.3284	4.343		1.427	2.918
	80	32.03	48.50	19.47	0.3738	4.032		1.507	2.525

[a] φ_L is the volume fraction of hydrophobic alkyl chains in surfactant molecule; a_0 is the lattice parameters of ILC phase; d_H is the radius of cylinder unit in H_1 phase; d_L is the thickness of hydrophobic domain in L_α phase; d_W is the thickness of water channel in ILC phase.

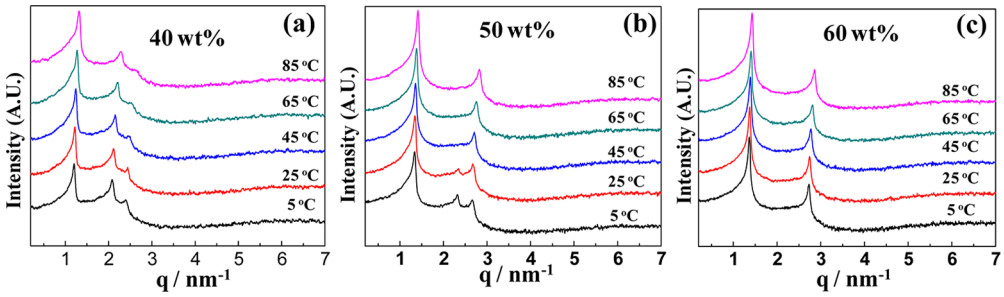

Figure 3. SAXS spectra for the (a) 40, (b) 50, and (c) 60 wt % samples with increasing temperature.

Scheme 1. Schematic Illustration of the Strategy for Preparation of Nanostructured Proton-Transporting Films

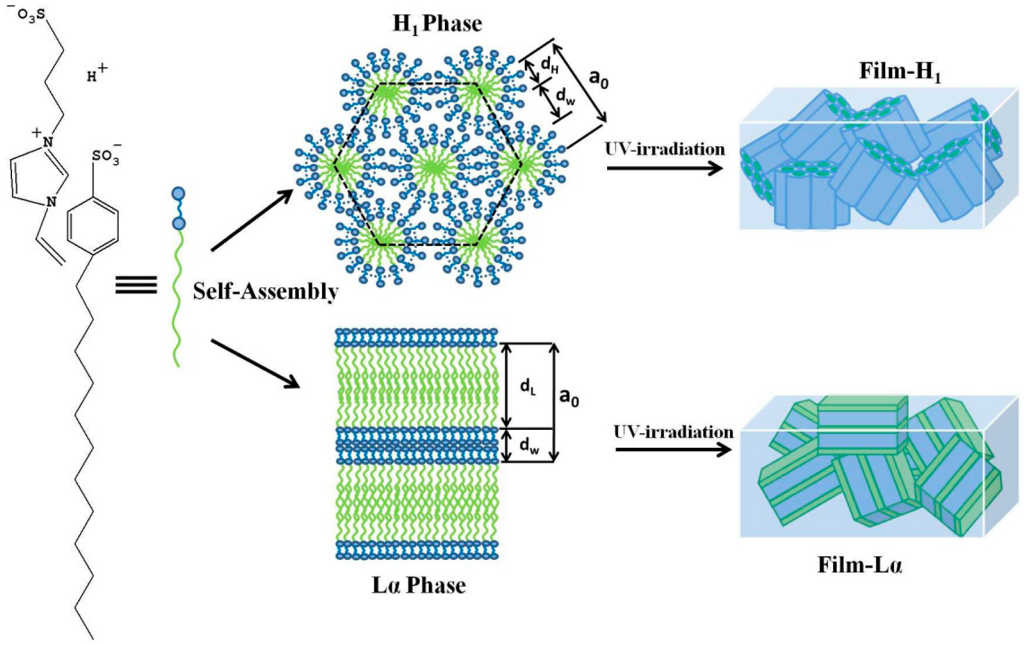

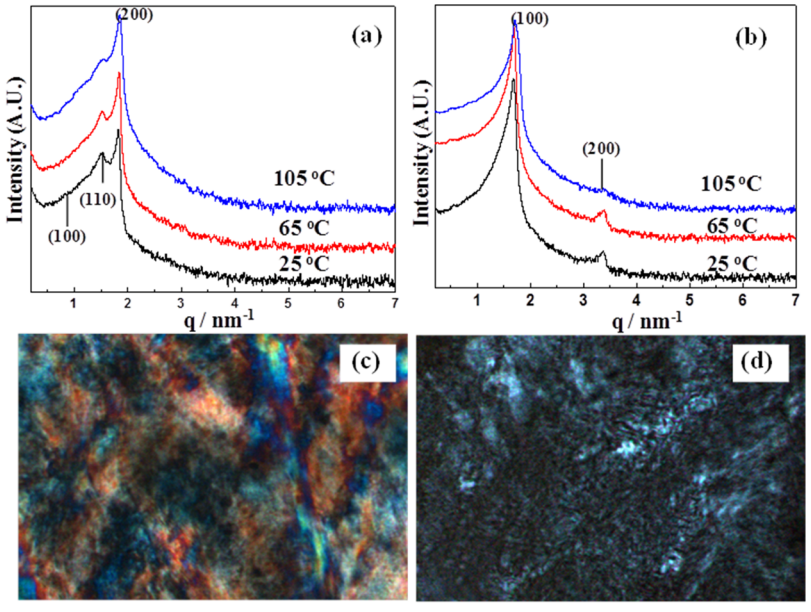

Figure 4. SAXS patterns of (a) Film-H_1 obtained by photopolymerization of VIPS−DBSA in H_1 phase and (b) Film-L_α obtained by photopolymerization of VIPS−DBSA in L_α phase. The SAXS data were collected at different temperatures. POM images of Film-H_1 (c) and Film-L_α (d) at 25 °C, respectively.

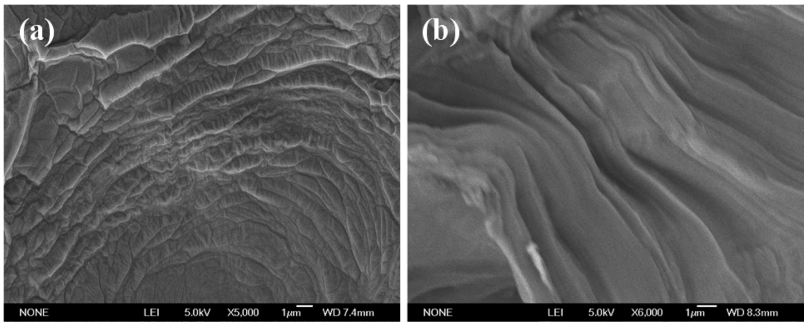

Figure 5. Scanning electron micrographs of the cross sections for (a) Film-H_1 and (b) Film-L_α.

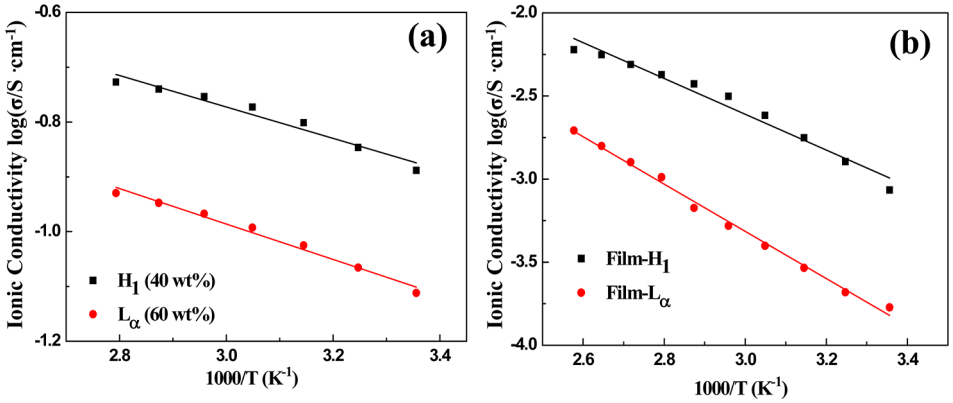

Figure 6. (a) Arrhenius plots of ionic conductivity for the VIPS−DBSA aqueous mixture in H_1 phase (black squares) and in L_α phase (red circles); (b) Arrhenius plots of ionic conductivity for the Film-H_1 (black squares) and Film-L_α (red circles).

equilibrated with 40 and 60 wt % of VIPS−DBSA aqueous mixture. Subsequently, the UV irradiation of the corresponding ILC sample in the presence of photoinitiator was conducted by a UV arc lamp around 365 nm with an intensity of 9 mW/cm^2 for 2 h at room temperature. The photopolymerization of VIPS−DBSA in hexagonal and lamellar phases has given two types of transparent free-standing polymeric films as Film-H_1 and Film-L_α. To determine the polymerization process, we conducted FT-IR spectroscopy to monitor the intensity of C═C stretching bands at ∼1650 cm^{-1} and C−H stretching bands at ∼920 cm^{-1}.[37] In the case of the ILC phase, D_2O should be used to replace H_2O to avoid the strong overlapping H−O−H band at ∼1600 cm^{-1}.[38] As shown in Figure S2 (Supporting Information), the intensities of IR bands at ∼1650 and ∼920 cm^{-1} significantly decrease for the Film-H_1 and Film-L_α after photopolymerization, which indicates that the cross-linking reaction occurs.

SAXS technique was applied to confirm the preservation of ILC nanostructures after photoirradiation. As shown in Figure 4, the SAXS pattern of Film-H_1 at 25 °C shows the typical Bragg peaks assigned to (100), (110), and (200) reflections of a hexagonal structure. The Film-L_α polymerized in the lamellar state also exhibits two peaks indexed as (100) and (200) reflections of a lamellar structure. The SAXS spectra support that the ILC nanostructures have been retained in the polymeric film during photopolymerization. The stability of the nanostructures in the cross-linked ILC phase was also examined by SAXS at different temperatures. The SAXS patterns of Film-H_1 and Film-L_α at 105 °C higher than the boiling point of water still show their typical Bragg peaks. This result demonstrates that the nanostructures of ILC fixed by photopolymerization are generally retained at a higher temperature region. Figure 4c,d shows the POM images of Film-H_1 and Film-L_α samples at 25 °C, respectively. The birefringence patterns for the two solid film samples were still observed after polymerization. The POM images of Film-H_1 and Film-L_α at higher temperature were also collected and shown in the Supporting Information.

The lattice parameter a_0 was also calculated on the basis of the SAXS data. The value of a_0 for Film-H_1 is 8.078 nm, which is much higher than that of the H_1 phase (5.939 nm in Table 1) containing 40 wt % VIPS−DBSA before photo cross-linking. However, the value of a_0 for Film-L_α reduces to 3.746 nm compared with the L_α phase (4.574 nm in Table 1) fabricated by 60 wt % VIPS−DBSA aqueous mixture. The polymerizable ethylenic bonds are located among the hydrophilic head groups and the cross-linking between these ethylenic bonds can result in an increase of the effective area of headgroups. The expansion of the cylinder unit cell can be rationalized by the enlargement of headgroups. For the L_α phase, the surfactant molecules show paratactic alignment, and so, the cross-linking of headgroup causes a more dense packing of the surfactant, resulting in the contraction of the lamellar unit cell.[39,40] Additionally, the variation in lattice parameter of H_1 phase is more pronounced than that of L_α phase due to the more interfacial curvature of monolayer cylinder aggregates.

To examine the nanostructures of the polymeric films on larger size scales, scanning electronic microscopy (SEM) was applied to analyze the bulk morphology of Film-H_1 and Film-L_α. Figure 5 shows the SEM images of cross sections for the two films. For SEM analysis, water must be removed, which may cause the polymer structure to collapse. However, the morphology of films should still show difference if the nanostructure is present.[41,42] Specifically, the SEM image of

Film-H_1 shown in Figure 5a exhibits defined cylindrical structures and the micrograph of Film-L_α shown in Figure 5b contains directed sheet-like structures. This structural information on SEM images directly parallels the above SAXS data.

Ionic Conductivity of the Films with Proton-Transporting Nanochannels. The phase behavior of the VIPS−DBSA aqueous mixture can be taken as a guideline for the study of proton-transporting behavior. We expect that the information on water channels in ILC phases can act as proton pathways and have significantly positive influence on the proton-transporting mechanism. First, we measured the ionic conductivities of the VIPS−DBSA aqueous mixture by an alternating current impedance method. As shown in Figure 6a, the ionic conductivities of the samples in both H_1 and L_α phase increase with the increasing temperature from 25 to 85 °C. The ionic conductivity of the sample with 40 wt % VIPS−DBSA in H_1 state is 0.129 S/cm at 25 °C and reaches to 0.187 S/cm at 85 °C. The sample with 60 wt % VIPS−DBSA in L_α state also exhibits an increasing ionic conductivity from 0.077 to 0.117 S/cm within the temperature range of 25−85 °C. Due to the sensitivity of ILC phases to the water content, the operation temperature cannot exceed 100 °C in order to avoid the water boiling. While for the cross-linking polymeric Film-H_1 and Film-L_α, the ionic conductivities can be measured at temperatures higher than 100 °C because the nanostructures of ILC fixed in the films are generally retained at a higher temperature region. Figure 6b shows the ionic conductivities of Film-H_1 and Film-L_α in a temperature range of 25−115 °C. The ionic conductivity of Film-H_1 varies from 8.51×10^{-4} to 6.02×10^{-3} S/cm and the ionic conductivity of Film-L_α increases from 1.07×10^{-4} to 1.95×10^{-3} S/cm with the increasing temperature. Although Film-H_1 and Film-L_α have different unit structures in film matrix, the ionic conductivities of the two films are still in the same order of magnitude because they both form low-dimensional hydrophilic channels for proton transport. It should be noted that the ionic conductivities of the solid polymeric films are lower than those of the samples in ILC state. Generally, the cross-linking of molecules can suppress the diffusion of molecules themselves and lead to the decrease in ionic conductivity.[20,43] However, the ionic conductivities of these nanostructured films are still 1−2 orders of magnitude higher than that of another electrolyte membrane Nafion 117.[44] This interesting phenomenon indicates that the topological structures of ILC phase fixed in the polymeric films play a chief role for the efficient proton transportation. We proposed that the proton transporting occurs in the hydrophilic part of VIPS−DBSA. So it is reasonable to consider the water channels as proton-transporting pathways. To better understand the proton-transporting mechanism, the activation energies of Film-H_1 and Film-L_α were calculated from the Arrhenius plots of ionic conductivity. The activation energies of Film-H_1 and Film-L_α are 8.96 and 11.82 kJ/mol, respectively. It is noted that the activation energy of water-swelled Nafion is approximate 15 kJ/mol.[45,46] The decrease in activation energy is believed to generate from the introduction of highly ordered topological structures within the polymer matrix. It is noteworthy to mention that there are two different ion-transporting mechanisms, vehicle and Grotthuss mechanisms. The vehicle mechanism is controlled by ion diffusion with a small value of conductivity,[47] while the Grotthuss mechanism is generated by ion hopping with high conducvitity.[48] When the protons are transported on the surface of the cylinder or layer unit, proton hopping always occurs through the hydrogen bond networks of headgroups,[27] while for the protons transported in the continuous water medium among cylinder or layer unit, diffusion controlled transport (vehicle) is the main mechanism. We proposed that the ion transport in Film-H_1 and Film-L_α consists of a series of hopping within cylinder or layer units and diffusion through water medium among cylinder or layer units. Thus, the more ordered nanostructures in Film-H_1 and Film-L_α can provide more ionic conduction pathways for proton hopping, resulting in a higher conductivity and lower activation energy.

CONCLUSIONS

In summary, we have successfully constructed proton-transporting ILC phases by a polymerizable imidazolium-type zwitterion and a kind of organic acid. The obtained hexagonal phase and lamellar phase can be retained by in-phase photopolymerization of ILC. The vinyl group in imidazolium-type zwitterions as a polymerizable moiety is the key in the cross-linking of the ILC topological structures. The polymerized Film-H_1 and Film-L_α with nanostructured channels have higher ionic conductivities and lower activation energies than the common electrolyte membrane Nafion 117. The present work shows a facile method to construct a nanostructured solid state film for proton-transporting membrane materials.

ASSOCIATED CONTENT

Supporting Information

SAXS patterns for 30, 70, and 80 wt % VIPS−DBSA aqueous mixtures with increasing temperatures; FT-IR spectra for the Film-H_1 and Film-L_α before and after photopolymerization; schematic illustration for H_1 and L_α phase of VIPS−DBSA aqueous mixture; POM images of Film-H_1 and Film-L_α at high temperature; indexing of the SAXS data of ILC phases, Film-H_1 and Film-L_α at 25 °C; theories and equations for calculation of the structural parameters of ILC phases; and equation for calculation of ionic conductivity and the dimensions of Film-H_1 and Film-L_α. This material is available free of charge via the Internet at http://pubs.acs.org.

AUTHOR INFORMATION

Corresponding Author

*E-mail: lqzheng@sdu.edu.cn. Phone: +86-531-88361528. Fax: +86-531-88564750.

Notes

The authors declare no competing financial interest.

ACKNOWLEDGMENTS

The authors are grateful to the National Basic Research Program (2013CB834505), the National Natural Science Foundation of China (No.91127017), the Specialized Research Fund for the Doctoral Program of Higher Education of China (No.20120131130003) and the Shandong Provincial Natural Science Foundation, China (ZR2012BZ001).

REFERENCES

(1) Savadogo, O. Emerging Membranes for Electrochemical Systems: (I) Solid Polymer Electrolyte Membranes for Fuel Cell Systems. *J. New Mater. Electrochem. Syst.* **1998**, *1*, 47−66.

(2) Savadogo, O. Emerging Membranes for Electrochemical Systems: Part II. High Temperature Composite Membranes for Polymer Electrolyte Fuel Cell (PEFC) Applications. *J. Power Sources* **2004**, *127*, 135−161.

(3) Armand, M.; Endres, F.; MacFarlane, D. R.; Ohno, H.; Scrosati, B. Ionic-Liquid Materials for the Electrochemical Challenges of the Future. *Nat. Mater.* **2009**, *8*, 621−629.
(4) Horike, S.; Umeyama, D.; Inukai, M.; Itakura, T.; Kitagawa, S. Coordination-Network-based Ionic Plastic Crystal for Anhydrous Proton Conductivity. *J. Am. Chem. Soc.* **2012**, *134*, 7612−7615.
(5) Horike, S.; Umeyama, D.; Kitagawa, S. Ion Conductivity and Transport by Porous Coordination Polymers and Metal−Organic Frameworks. *Acc. Chem. Res.* **2013**, *46*, 2376−2384.
(6) Zhang, H.; Shen, P. K. Recent Development of Polymer Electrolyte Membranes for Fuel Cells. *Chem. Rev.* **2012**, *112*, 2780−2832.
(7) Mauritz, K. A.; Moore, R. B. State of Understanding of Nafion. *Chem. Rev.* **2004**, *104*, 4535−4585.
(8) Banerjee, S.; Curtin, D. E. Nafion® Perfluorinated Membranes in Fuel Cells. *J. Fluorine Chem.* **2004**, *125*, 1211−1216.
(9) Souzy, R.; Ameduri, B. Functional Fluoropolymers for Fuel Cell Membranes. *Prog. Polym. Sci.* **2005**, *30*, 644−687.
(10) Di Noto, V.; Piga, M.; Giffin, G. A.; Lavina, S.; Smotkin, E. S.; Sanchez, J. Y.; Iojoiu, C. Influence of Anions on Proton-Conducting Membranes Based on Neutralized Nafion 117, Triethylammonium Methanesulfonate, and Triethylammonium Perfluorobutanesulfonate. 1. Synthesis and Properties. *J. Phys. Chem. C* **2012**, *116*, 1361−1369.
(11) Lu, F.; Gao, X. P.; Yan, X. J.; Gao, H. J.; Shi, L. J.; Jia, H.; Zheng, L. Q. Preparation and Characterization of Nonaqueous Proton-Conducting Membranes with Protic Ionic Liquids. *ACS Appl. Mater. Interfaces* **2013**, *5*, 7626−7632.
(12) Binnemans, K. Ionic Liquid Crystals. *Chem. Rev.* **2005**, *105*, 4148−4204.
(13) Zhao, M. W.; Gao, Y. A.; Zheng, L. Q. Liquid Crystalline Phases of the Amphiphilic Ionic Liquid *N*-hexadecyl-*N*-methylpyrrolidinium Bromide Formed in the Ionic Liquid Ethylammonium Nitrate and in Water. *J. Phys. Chem. B* **2010**, *114*, 11382−11389.
(14) Zhang, S. H.; Yuan, J.; Ma, H. C.; Li, N.; Zheng, L. Q.; Inoue, T. Aqueous Phase Behavior of Ionic Liquid-Related Gemini Surfactant Revealed by Differential Scanning Calorimetry and Polarized Optical Microscopy. *Colloid Polym. Sci.* **2011**, *289*, 213−218.
(15) Shi, L. J.; Zhao, M. W.; Zheng, L. Q. Lyotropic Liquid Crystalline Phases Formed in Ternary Mixtures of *N*-alkyl-*N*-methylpyrrolidinium Bromide/1-Decanol/Water. *RSC Adv.* **2012**, *2*, 11922−11929.
(16) Mukai, T.; Yoshio, M.; Kato, T.; Yoshizawa, M.; Ohno, H. Anisotropic Ion Conduction in A Unique Smectic Phase of Self-Assembled Amphiphilic Ionic Liquids. *Chem. Commun.* **2005**, *10*, 1333−1335.
(17) Yoshio, M.; Mukai, T.; Kanie, K.; Yoshizawa, M.; Ohno, H.; Kato, T. Layered Ionic Liquids: Anisotropic Ion Conduction in New Self-Organized Liquid-Crystalline Materials. *Adv. Mater.* **2002**, *14*, 351−354.
(18) Ichikawa, T.; Yoshio, M.; Hamasaki, A.; Taguchi, S.; Liu, F.; Zeng, X.; Ungar, G.; Ohno, H.; Kato, T. Induction of Thermotropic Bicontinuous Cubic Phases in Liquid-Crystalline Ammonium and Phosphonium Salts. *J. Am. Chem. Soc.* **2012**, *134*, 2634−2643.
(19) Kerr, R. L.; Miller, S. A.; Shoemaker, R. K.; Elliott, B. J.; Gin, D. L. New Type of Li Ion Conductor with 3D Interconnected Nanopores via Polymerization of a Liquid Organic Electrolyte-Filled Lyotropic Liquid-Crystal Assembly. *J. Am. Chem. Soc.* **2009**, *131*, 15972−15973.
(20) Yoshio, M.; Kagata, T.; Hoshino, K.; Mukai, T.; Ohno, H.; Kato, T. One-Dimensional Ion-Conductive Polymer Films: Alignment and Fixation of Ionic Channels Formed by Self-Organization of Polymerizable Columnar Liquid Crystals. *J. Am. Chem. Soc.* **2006**, *128*, 5570−5577.
(21) Ichikawa, T.; Yoshio, M.; Hamasaki, A.; Kagimoto, J.; Ohno, H.; Kato, T. 3D Interconnected Ionic Nano-Channels Formed in Polymer Films: Self-Organization and Polymerization of Thermotropic Bicontinuous Cubic Liquid Crystals. *J. Am. Chem. Soc.* **2011**, *133*, 2163−2169.
(22) Zhang, H.; Li, L.; Möller, M.; Zhu, X.; Rueda, J. J. H.; Rosenthal, M.; Ivanov, D. A. From Channel-Forming Ionic Liquid Crystals Exhibiting Humidity-Induced Phase Transitions to Nanostructured Ion-Conducting Polymer Membranes. *Adv. Mater.* **2013**, *25*, 3543−3548.
(23) Gao, X. P.; Lu, F.; Shi, L. J.; Jia, H.; Gao, H. J.; Zheng, L. Q. Nanostructured Aqueous Lithium-Ion Conductors Formed by the Self-Assembly of Imidazolium-Type Zwitterions. *ACS Appl. Mater. Interfaces* **2013**, *5*, 13312−13317.
(24) Ohno, H.; Yoshizawa, M.; Ogihara, W. A New Type of Polymer Gel Electrolyte: Zwitterionic Liquid/Polar Polymer Mixture. *Electrochim. Acta* **2003**, *48*, 2079−2083.
(25) Yoshizawa, M.; Ohno, H. Anhydrous Proton Transport System Based on Zwitterionic Liquid and HTFSI. *Chem. Commun.* **2004**, *16*, 1828−1829.
(26) Tiyapiboonchaiya, C.; Pringle, J. M.; Sun, J.; Byrne, N.; Howlett, P. C.; Macfarlane, D. R.; Forsyth, M. The Zwitterion Effect in High-Conductivity Polyelectrolyte Materials. *Nat. Mater.* **2004**, *3*, 29−32.
(27) Ueda, S.; Kagimoto, J.; Ichikawa, T.; Kato, T.; Ohno, H. Anisotropic Proton-Conductive Materials Formed by the Self-Organization of Phosphonium-Type Zwitterions. *Adv. Mater.* **2011**, *23*, 3071−3074.
(28) Ichikawa, T.; Kato, T.; Ohno, H. 3D Continuous Water Nanosheet as a Gyroid Minimal Surface Formed by Bicontinuous Cubic Liquid-Crystalline Zwitterions. *J. Am. Chem. Soc.* **2012**, *134*, 11354−11357.
(29) Soberats, B.; Yoshio, M.; Ichikawa, T.; Taguchi, S.; Ohno, H.; Kato, T. 3D Anhydrous Proton-Transporting Nanochannels Formed by Self-Assembly of Liquid Crystals Composed of a Sulfobetaine and a Sulfonic Acid. *J. Am. Chem. Soc.* **2013**, *135*, 15286−15289.
(30) Kerr, R. L.; Miller, S. A.; Shoemaker, R. K.; Elliott, B. J.; Gin, D. L. New Type of Li Ion Conductor with 3D Interconnected Nanopores via Polymerization of a Liquid Organic Electrolyte-Filled Lyotropic Liquid-Crystal Assembly. *J. Am. Chem. Soc.* **2009**, *131*, 15972−15973.
(31) Fujita, M. Y.; Byrne, N.; Forsyth, M.; MacFarlane, D. R.; Ohno, H. Proton Transport Properties in Zwitterion Blends with Brønsted Acids. *J. Phys. Chem. B* **2010**, *114*, 16373−16380.
(32) Carr, L.; Cheng, G.; Xue, H.; Jiang, S. Engineering the Polymer Backbone to Strengthen Nonfouling Sulfobetaine Hydrogels. *Langmuir* **2010**, *26*, 14793−14798.
(33) Zhang, J.; Dong, B.; Zheng, L. Q.; Li, N.; Li, X. W. Lyotropic Liquid Crystalline Phases Formed in Ternary Mixtures of 1-Cetyl-3-Methylimidazolium Bromide/p-Xylene/Water: A SAXS, POM, and Rheology Study. *J. Colloid Interface Sci.* **2008**, *321*, 159−165.
(34) Zhao, Y.; Chen, X.; Wang, X. Liquid Crystalline Phases Self-Organized from a Surfactant-like Ionic Liquid C_{16}mimCl in Ethylammonium Nitrate. *J. Phys. Chem. B* **2009**, *113*, 2024−2030.
(35) Wang, X.; Chen, X.; Zhao, Y.; Yue, X.; Li, Q.; Li, Z. Nonaqueous Lyotropic Liquid-Crystalline Phases Formed by Gemini Surfactants in a Protic Ionic Liquid. *Langmuir* **2012**, *28*, 2476−2484.
(36) Lux, G. G.; Donnio, B.; Heinrich, B.; Krafft, M. P. Thermal Behavior and High- and Low-Temperature Phase Structures of Gemini Fluorocarbon/Hydrocarbon Diblocks. *Langmuir* **2013**, *29*, 5325−5336.
(37) Hoag, B. P.; Gin, D. L. Cross-Linkable Liquid Crystal Monomers Containing Hydrocarbon 1,3-Diene Tail Systems. *Macromolecules* **2000**, *33*, 8549−8558.
(38) Pindzola, B. A.; Hoag, B. P.; Gin, D. L. Polymerization of a Phosphonium Diene Amphiphile in the Regular Hexagonal Phase with Retention of Mesostructure. *J. Am. Chem. Soc.* **2001**, *123*, 4617−4618.
(39) Pindzola, B. A.; Jin, J.; Gin, D. L. Cross-Linked Normal Hexagonal and Bicontinuous Cubic Assemblies via Polymerizable Gemini Amphiphiles. *J. Am. Chem. Soc.* **2003**, *125*, 2940−2949.
(40) Odian, G. *Principles of Polymerization*, 3rd ed.; John Wiley & Sons: New York, 1991.
(41) Forney, B. S.; Baguenard, C.; Guymon, C. A. Effects of Controlling Polymer Nanostructure Using Photopolymerization within Lyotropic Liquid Crystalline Templates. *Chem. Mater.* **2013**, *25*, 2950−2960.
(42) Zhang, J.; Xie, Z.; Hill, A. J.; She, F. H.; Thornton, A. W.; Hoang, M.; Kong, L. X. Structure Retention in Cross-Linked

Poly(ethylene glycol) Diacrylate Hydrogel Templated from a Hexagonal Lyotropic Liquid Crystal by Controlling the Surface Tension. *Soft Matter* **2012**, *8*, 2087−2094.
(43) Ogihara, W.; Washiro, S.; Nakajima, H.; Ohno, H. Effect of Cation Structure on the Electrochemical and Thermal Properties of Ion Conductive Polymers Obtained From Polymerizable Ionic Liquids. *Electrochim. Acta* **2006**, *51*, 2614−2619.
(44) Sood, R.; Iojoiu, C.; Espuche, E.; Gouanvé, F.; Gebel, G.; Mendil-Jakani, H.; Lyonnard, S.; Jestin, J. Proton Conducting Ionic Liquid Doped Nafion Membranes: Nano-Structuration, Transport Properties, and Water Sorption. *J. Phys. Chem. C* **2012**, *116*, 24413−24423.
(45) Siroma, Z.; Kakitsubo, R.; Fujiwara, N.; Ioroi, T.; Yamazaki, S.; Yasuda, K. Depression of Proton Conductivity in Recast Nafion® Film Measured on Flat Substrate. *J. Power Sources* **2009**, *189*, 994−998.
(46) Baek, J. S.; Park, J. S.; Sekhon, S. S.; Yang, T. H.; Shul, Y. G.; Choi, J. H. Preparation and Characterisation of Non-aqueous Proton-Conducting Membranes with the Low Content of Ionic Liquids. *Fuel Cells* **2010**, *10*, 762−769.
(47) Kreuer, K.-D.; Rabenau, A.; Weppner, W. Vehicle Mechanism, A New Model for the Interpretation of the Conductivity of Fast Proton Conductors. *Angew. Chem., Int. Ed.* **1982**, *21*, 208−209.
(48) Kreuer, K.-D.; Paddison, S. J.; Spohr, E.; Schuster, M. Transport in Proton Conductors for Fuel-Cell Applications: Simulations, Elementary Reactions, and Phenomenology. *Chem. Rev.* **2004**, *104*, 4637−4678.